Arrangement of the Acetylcholine Receptor Subunits in the Resting and Desensitized States, Determined by Cryoelectron Microscopy of Crystallized *Torpedo* Postsynaptic Membranes

Nigel Unwin, Chikashi Toyoshima, and Elizabeth Kubalek

Department of Cell Biology, Stanford University Medical School, Stanford, California 94305

Abstract. Two conformational states of the nicotinic acetylcholine receptor have been investigated by cryoelectron microscopy of flattened vesicular crystals grown from *Torpedo marmorata* postsynaptic membranes. One was obtained from the vesicles without acetylcholine present, and is presumed to correspond to the native, or resting state; the other was obtained from the vesicles after exposure to 100 μM to 5 mM carbamylcholine (an acetylcholine analogue) and is presumed to correspond to a desensitized state. Both conformations were determined in three-dimensions to a resolution of 18 Å, sufficient to reveal the configurations of the five subunits around the central ion channel over most of their length.

The subunits of either structure have a similar appearance, consistent with their amino acid homology. They are each aligned almost parallel to the axis of the receptor, conferring a high degree of pentagonal symmetry to the bilayer portion and a contiguous region on the synaptic side. Their external surfaces form a pronounced ridge in the bilayer portion, which broadens toward the synaptic end.

Comparison of features in the two three-dimensional maps reveals that carbamylcholine induces a quaternary rearrangement, involving predominantly the δ-subunit. The densities corresponding to this subunit are tilted by ~10° tangential to the axis of the receptor over a large fraction of its length, and become misaligned relative to the densities corresponding to the other four subunits. The γ-subunit is also affected, being displaced slightly away from the axis of the receptor. The α- and β-subunits may be affected on a more localized scale. The overall changes are most pronounced in the synaptic region, where the ligand-binding site is located, and in the cytoplasmic region, which may be closer to the gate of the channel. The physiological process of desensitization appears to be associated with a structural transition in which the subunits switch to a less symmetrical configuration.

THE nicotinic acetylcholine receptor is a pentameric membrane protein composed of four different but homologous polypeptide chains, arranged in the order α, β, α, γ, δ (14, 25) around a central water-filled channel. It is organized in high concentrations in the postsynaptic membranes of electrically excitable cells, where it responds to the neurotransmitter, acetylcholine, released into the synaptic cleft. Within a millisecond of acetylcholine binding, the receptor creates a transient pathway across the membrane for small cations to diffuse. On continued exposure to this ligand, however, the receptor may become inactivated and block further ion flux across the membrane, a process known as desensitization. The desensitized receptor, like other inactivated membrane channels, has a conformation which is distinct from that of the receptor in its unoccupied, or resting state.

The differences between the resting and desensitized states have not hitherto been explored by direct structural methods, although the transition has been examined extensively by chemical kinetic measurements (19). Changes in fluorescence of extrinsic probes and of intrinsic tryptophan residues have also been correlated with the two states (3, 13). The subunits participating include the α-subunits, which contain the acetylcholine binding sites, and the γ- and δ-subunits, which when phosphorylated in vitro by cAMP-dependent protein kinase, increase markedly the desensitization rate (21). Additional evidence that phosphorylation of the δ-subunit influences the kinetics of desensitization has been obtained from recent in vivo studies (26).

In the present study we investigate the two conformations using receptors crystallized from isolated postsynaptic membranes in the form of long, tubular vesicles (5). An earlier analysis of the tubular crystals by cryoelectron microscopy had revealed the pseudo-pentagonal three-dimensional structure of the receptor at 25 Å resolution (6). Subsequently, the locations were determined of the individual polypeptide chains (25). Here we extend the three-dimensional analysis to a resolution of ~18 Å by the use of a cold stage of improved design and by correcting the images for small dis-

Nigel Unwin's and Chikashi Toyoshima's current address is MRC Laboratory of Molecular Biology, Hills Road, Cambridge CB2 2GH, United Kingdom.

tortions of the crystal lattice (17). We obtain two independent maps, corresponding to the receptors before and after prolonged exposure to the acetylcholine analogue, carbamylcholine. These maps confirm the basic features of the receptor seen at lower resolution previously, and lead to a qualitative description of a change in conformation presumed to correspond to desensitization. Most clearly revealed at this resolution are small rearrangements involving the γ- and δ-subunits.

Materials and Methods

Materials

Tubular crystals of acetylcholine receptor were obtained from the electric organ of *Torpedo marmorata* (Marine Station, Arcachon, France) in the presence of protease inhibitors, as described (5). They were kept in 100 mM sodium cacodylate buffer (pH 6.8). Carbamylcholine chloride was from Sigma Chemical Co. (St. Louis, MO).

Specimen Preparation

Carbon support films were prepared by overlaying copper grids (400 mesh; E.F. Fullam, Inc., Schenectady, NY) with collodion film, evaporating carbon onto this film and dissolving the plastic away with amyl acetate. They were pretreated within 1 h of use by glow discharge in the presence of amylamine vapor (10) and taken to a cold room, maintained at 4°C and close to 100% humidity, for subsequent steps. 5-μl aliquots of solution containing the tubular crystals were applied to each grid, incubated (1 min), and blotted (~4 s), using dried Whatman No. 1 filter paper to remove the excess. The grids were immediately frozen by plunging into liquid ethane slush (−160°C) and, later, stored under liquid nitrogen until ready for examination. To obtain desensitized receptors, the tubes were exposed to carbamylcholine at least several minutes before freezing.

The above preparation conditions caused complete flattening of most tubes against the carbon support, allowing their two sides to be analyzed as if they were planar two-dimensional crystals.

Electron Microscopy

Images were recorded at 120 KV, using a Philips EM400T electron microscope equipped with a low dose kit and an auxiliary twin-bladed anticontaminator. The temperature of the specimen was maintained at −168°C using a prototype Gatan Mk.2 cryo-holder connected to a temperature regulator. Goniometer tilt angles were restricted to ±15° for maximum imaging stability. Higher specimen tilts were achieved by mounting the grids onto an 8° wedge (for intermediate tilt angles) or by cutting the grids under liquid nitrogen and kinking their central portion symmetrically to produce a V-shaped profile.

Suitable areas on the grids were located at a magnification of 2,800×, using a beam of ~1 cm diam on the phosphor viewing screen; focusing, astigmatism, and drift compensation (by adjustment of the temperature regulator) were performed at a nominal magnification of 170,000× on an area along the tilt axis adjacent to the one of interest; images were recorded at a calibrated magnification (36) of 56,300×, using an underfocus value of 8,000–9,000 Å and a beam diameter about equal to that of the small dimension of the film. Appropriate height adjustments were made to the goniometer stage to maintain the objective lens current for recording at 6.15 ± 0.02 A, so that the magnification varied by no more than 0.3%. The photographs were obtained in low dose/high dose pairs (35) to reveal most clearly both the structure (first photograph) and the information needed to establish the level of defocus and angle of view (second photograph). Exposure of the low dose image was for 1 s at a total dose of ~20 electrons/Å^2; exposure of the high dose image was for 2 s, after irradiating to sublimate most of the ice. The film (Kodak S0163) was developed for 10 min in Kodak D19 developer.

Preliminary Selection

Micrographs were evaluated initially by optical diffraction. They were retained for further analysis if, in the first of the pair, the diffraction patterns from both sides of the tube were sharp and strong, contained no major overlapping reflections, and were superimposed on a background in which the pattern of concentric rings (32) associated with the contrast transfer function (CTF)[1] was equally visible in all directions. In addition, the position in the CTF of the first zero was required to be at a resolution of around 17 Å to minimize differences in optical character between one image and the next. This necessitated that the defocus, δf, be within a narrow range (7,000 Å < δf <9,500 Å). Accurate values for the position of the first zero (and defocus) were obtained by densitometry of the area of tube selected and sector averaging, as described below.

The second micrograph of the pair needed to be of sufficient quality to define the defocus accurately (±250 Å) in four well separated regions. Typically, the optical diffraction patterns from such a micrograph would display several CTF rings extending to a resolution of ~8 Å.

Data Collection

Areas of tubes in the low dose micrographs, selected according to the above criteria, were converted into digital form using a Perkin Elmer PDS flatbed microdensitometer operated with a scanning aperture and step size of 25 μm. They were analyzed, one side at a time, essentially as described (5, 6, 25). The standard array size for the Fourier transform and lattice correction calculations was 1,500 × 500, and the area of tube analyzed was typically 5,000 Å by 1,000 Å (i.e., ~2 × 400 unit cells; see Table I). The filter mask used in the lattice correction procedure and the correlation coefficient cut-off for applying the corrections (0.15) were the same as previously (25), and such as to exclude from the corrections areas of the tube where the lattice was rotated more than ~2° from the average. The corrections were effective for most tubes over at least 80% of the length selected. In some instances, particularly with the narrower tubes, variation across the filtered image indicated that the side concerned was not flat; in such cases the processing was abandoned. The correction for lattice distortions, applied to the remaining data, gave more substantial improvements than with the negatively stained tubes (25), increasing the number of reflections above background by a factor of almost two.

Areas in the high dose micrographs were desitometered as above to create 512 × 512 digitized arrays centered about four orthogonally arranged points. Defocus values were determined by matching the CTF ring patterns displayed in Fourier transforms of these arrays against a set of simulated patterns, computed according to the magnification and electron optical conditions used, and at defocus intervals of 250 Å. Alternatively, radial plots of the CTF maxima and minima were calculated by sector averaging of the rings, and the defocus values were estimated by comparison with theory; both methods yielded similar results. Based on this information, and the position of the tube in relation to the four orthogonally arranged points, we could estimate the magnitude and direction of tilt (6). The errors inherent in this method of establishing the tilt parameters were up to ±2° in the magnitude and ±4° in the direction of tilt, according to the range of the values obtained for the four possible planes, each defined by only three of the points. The alternative geometric method of establishing the tilt parameters (1), which relies on apparent distortion of the crystal lattice, was less appropriate because of variations in lattice parameters from one tube to the next (see Table I).

Combining Images of Tilted Specimens

The sides of tubes each provided separate data for combining with others to create the three-dimensional Fourier terms. The data consisted of the integrated, background-corrected amplitudes, phases and quality indicators (17) for all (h, k) points on the reciprocal net to a resolution of 18 Å, after processing as above. Of these points, typically 20–30 represented reflections with peak amplitudes greater than twice the local background level.

The data were combined according to the symmetry of the two-sided plane group p2 (5) and with a distance for amplitude and phase comparison along the lattice lines of 1/400 Å^{-1}. Reflections with peak amplitudes less than twice the local background level were excluded from the comparisons. Initially, the combining was done cumulatively, with the averaged projection data (Table I) as the reference set and the remaining data added in order of increasing tilt (1, 18). Each new image was thus assigned a phase origin and scale factor to give the best possible agreement with the previously processed images. Several images for which the average phase error or R factor (see Table II) was unusually high were eliminated at this stage, it being assumed that they contained defective lattices or were not of uniform quality in all directions. Subsequently, each dataset was refined by comparison of each image against all the others, phase shifted and scaled according

1. *Abbreviation used in this paper*: CTF, contrast transfer function.

Table I. Projection Data

Native tubes							Carbamylcholine-treated tubes						
a	b	γ*	Unit cells	Defocus cut-off‡	N§	Phase error‖	a	b	γ	Unit cells	Defocus cut-off	N	Phase error
⌜88.48¶	154.80	119.97	543	17.2	32	21.4	⌜94.51	163.15	118.05	504	16.3	36	20.4
⌞88.31	154.33	119.53	533	17.2	35	19.6	⌞95.05	163.35	118.17	472	16.3	31	21.6
⌜91.26	165.28	118.85	400	17.5	34	10.9	⌜90.84	158.43	118.81	602	17.2	36	16.6
⌞90.97	164.15	118.24	348	17.5	37	17.4	⌞91.43	157.22	118.30	432	17.2	34	16.5
⌜92.28	163.01	119.86	437	18.1	33	18.1	⌜89.08	158.30	117.38	360	15.9	37	14.3
⌞91.45	162.20	119.06	442	18.1	35	20.1	⌞89.70	159.10	117.82	412	15.9	37	15.3
⌜91.74	161.31	118.51	412	16.9	35	18.1	⌜93.16	157.51	119.35	351	16.9	34	11.2
⌞92.63	161.73	119.01	372	16.9	34	18.0	⌞91.65	157.68	119.28	312	16.9	35	20.7
⌜85.89	155.39	117.66	516	16.5	38	17.1	⌜90.54	161.58	118.80	407	16.3	35	14.0
⌞86.06	156.25	118.14	540	16.5	38	11.2	⌞90.62	161.40	118.10	462	16.3	37	12.7
91.01	165.45	118.55	456	17.1	35	11.7	92.19	156.68	118.77	468	17.9	35	12.5
mean			454	17.2	35	16.7	mean			478	16.7	35	16.0

* Unit cell dimensions a, b in Å; included angle, γ in degrees.
‡ Resolution in Å of first zero in contrast transfer function.
§ Number of above-background reflections used in phase origin refinement; these include: (0, 2), (0, 3), (0, 4), (0, 5), (0, 6), (0, 7), (1, −7), (1, −6), (1, −5), (1, −4), (1, −3), (1, −2), (1, 0), (1, 2), (1, 3), (1, 4), (1, 5), (1, 6), (2, −6), (2, −5), (2, −4), (2, −3), (2, −2), (2, −1), (2, 0), (2, 3), (2, 4), (3, −7), (3, −5), (3, −4), (3, −3), (3, −1), (3, 0), (3, 1), (3, 2), (4, −6), (4, −4), (4, −2), (4, −1).
‖ Average error in degrees; based on comparison of individual phases with nearest centrosymmetric values.
¶ Brackets identify data from 2 sides of the same tube.

to the values determined in the previous step. These refined values of amplitude and phase were used to map out the continuous variations along each reciprocal lattice line, by means of a least squares curve-fitting program (2), with the amplitudes weighted according to the reliability of the corresponding phases. The continuous variations were then sampled at regular intervals (1/400 $Å^{-1}$) to provide the three-dimensional Fourier terms. Several lattice lines having weak amplitudes and essentially random phases were excluded from the refinement step and from subsequent calculations.

Calculation and Evaluation of the Structures

Maps were synthesized both directly and after compensating the amplitudes of the low resolution Fourier terms, lying within the first maximum (~1/25 $Å^{-1}$) of the CTF. The compensations were made by assuming the image to be that of a "weak phase-weak amplitude" object (11), and we used a figure of 0.15 for the maximum fraction of the total contrast contributed by amplitude contrast. This value provided about the same relative weighting to the low and high resolution terms as was obtained from receptors in negative stain (6). The value measured experimentally from the ice-embedded tubes was only 0.07 (33); however, we considered that compensation on this basis was less appropriate because it would give undue weight to the low resolution Fourier terms; these were already, in effect, enhanced almost two times as a result of radiation damage (33).

The influence of errors in the projection maps was assessed by applying the Students *t* test to measure the significance of differences (25). The procedure was to compare on a point-by-point basis a set of projection maps determined from several tubes (5–15) treated in one way (e.g., carbamylcholine absent) with a set of projection maps determined from several tubes treated in another way (e.g., carbamylcholine present). The *t* test measured the significance of the differences between the mean densities in either set, taking account of the standard deviations at each point. The three-dimensional maps were evaluated by dividing the original image datasets in two and comparing half-datasets which were processed independently.

To make quantitative comparisons between the native and carbamylcholine-treated receptors the maps were synthesized in the form of three-dimensional numerical arrays. Volumes consisting of 45 × 45 × 77 or 90 × 90 × 33 (x, y, z) pixels were boxed off around single molecules and used for further calculations. Radial projections were obtained by interpolating the arrays to generate a set of equally spaced cylindrical sections concentric about the receptor axis, and then superposing these sections on top of one another. The degree of fivefold symmetry at various levels through the two maps was measured by Fourier processing (9) of successive (x, y) sections.

Absolute Hand

The absolute hand of the structure was established in an earlier study by determining from tilting experiments which side of the tube was uppermost (i.e., nearest the electron source), and observing that the synaptic end of the receptor protruded from the outer surface (5). However, the structure was subsequently visualized only in projection or in three-dimensions at very low resolution, insufficient to identify distinguishing features of individual subunits. In this paper, features of the individual subunits are distinguished and have a chirality, the sense of which is relevant to the descriptions given. We therefore reevaluated the handedness more directly, using heavy metal shadowing to visualize the outer surface of the tube. Photographs (Fig. 1) confirmed that (*a*) the side nearest the electron source is the one in which the near-axial row of close-packed receptors points in a clockwise, rather than anticlockwise sense relative to the tube axis (see Fig. 9 *a* of reference 5), and that (*b*) the synaptic end of the receptor (forming the prominent annular entrance of the channel [6]) protrudes outwards. Thus all our descriptions of the receptor are presented with the correct absolute hand.

Position of Bilayer

The alignment of the bilayer with respect to the structural details was established by comparing the present data with data from a previous study (6) in which the bilayer was located by correlating maps from tubes embedded both in ice and in stain (see Fig. 2). For the two present maps, the average differences in phase along the lattice lines was smallest with no change in the relative positions of their phase origins, indicating that their alignment is equivalent perpendicular to the plane of the bilayer. However, comparison of either map against the previous map shows that a relative shift of ~2° (i.e., 2 × 400/360 = 2.2 Å) is needed to minimize the phase differences. The position of the bilayer in the present maps is therefore equal to the previous position after correction for this shift.

Results

Pilot Experiments

Fig. 3 shows typical images from the native untilted ice-embedded tubes. No clear difference could be detected directly between such images and those from tubes to which carbamylcholine had been added. The diffraction patterns for the two cases were also very similar (Fig. 4). To determine if there were in fact genuine differences in receptor structure, we calculated sets of projection maps from images relating to various conditions and applied the statistical *t* test to compare the sets (see Materials and Methods). Using 4–6 such maps/set, it was found that tubes which had been ex-

Table II. Three-dimensional Data

Native tubes							Carbamylcholine-treated tubes						
Tilt angle	Tilt axis*	Unit cells	Defocus cut-off‡	N§	Phase error‖	R¶	Tilt angle	Tilt axis	Unit cells	Defocus cut-off	N	Phase error	R
4.7	90.2	444	16.1	27	10.0	0.16	5.4	5.2	341	17.1	30	9.3	0.20
4.7	12.2	384	16.1	28	13.5	0.27	5.5	20.3	630	16.5	32	13.9	0.21
7.5	121.6	390	17.9	27	8.1	0.22	5.5	83.4	630	16.5	29	11.9	0.18
7.5	161.8	442	17.9	26	9.9	0.21	11.2	142.1	336	16.5	29	23.9	0.21
10.0	7.4	456	18.0	31	16.3	0.19	10.3	10.3	290	16.4	28	13.2	0.20
12.9	97.5	385	16.4	28	10.4	0.18	11.0	38.4	330	17.4	30	12.7	0.16
10.0	90.4	546	18.0	27	17.3	0.18	11.0	72.0	370	17.4	28	15.2	0.21
12.9	0.9	374	16.4	26	9.0	0.21	9.8	118.2	396	17.6	29	16.1	0.22
10.3	69.4	387	17.2	27	19.0	0.33	9.8	166.9	403	17.6	27	16.5	0.33
15.1	84.0	410	17.7	20	10.7	0.23	12.4	88.0	364	18.1	27	14.4	0.31
15.1	7.0	390	17.7	20	8.8	0.26	12.4	19.0	351	18.1	22	14.3	0.29
16.4	0.4	390	18.8	23	12.0	0.25	15.2	7.1	418	16.5	25	9.1	0.34
16.4	108.5	380	18.8	23	11.2	0.31	15.2	118.0	462	16.5	31	11.0	0.21
18.3	96.2	405	16.1	23	14.4	0.30	16.0	143.1	320	16.2	17	10.5	0.22
18.3	6.3	396	16.1	27	13.2	0.27	16.0	142.8	360	16.2	25	18.9	0.29
18.6	120.0	440	16.2	23	13.2	0.36	20.2	153.1	336	16.8	25	17.2	0.25
18.6	162.2	451	16.2	25	7.8	0.26	21.1	141.6	444	16.7	24	16.4	0.23
18.3	125.0	420	15.5	28	14.4	0.25	21.1	146.2	432	16.7	29	13.1	0.22
18.3	164.7	510	15.5	33	12.7	0.23	20.9	130.6	429	16.1	24	15.1	0.39
17.9	47.6	436	17.9	23	9.6	0.27	19.9	101.8	432	17.8	18	12.0	0.35
17.9	62.6	438	17.9	19	12.5	0.28	19.9	173.2	432	17.8	18	15.6	0.33
18.4	14.0	413	16.4	25	17.4	0.32	22.2	46.9	384	15.9	20	17.7	0.32
18.4	96.0	399	16.4	27	15.2	0.37	22.2	58.0	408	15.9	15	18.3	0.38
19.6	141.2	492	16.3	29	6.2	0.25	21.5	111.8	348	17.3	22	17.3	0.44
19.6	139.8	504	16.3	27	13.3	0.23	20.8	65.5	368	17.0	24	19.9	0.29
19.0	71.2	374	17.5	16	18.6	0.36	20.8	27.5	377	17.0	23	23.0	0.36
19.0	33.1	287	17.5	20	12.5	0.40	21.1	59.9	312	16.8	18	17.1	0.44
24.2	14.5	403	16.2	19	9.3	0.33	23.8	105.4	280	16.3	23	23.8	0.37
24.2	84.8	408	16.2	19	7.9	0.35	23.8	172.4	266	16.3	21	16.3	0.30
26.5	157.0	518	18.1	21	19.7	0.41	24.9	146.6	429	17.6	22	9.7	0.25
25.6	159.6	380	17.6	19	25.1	0.22	24.9	139.2	492	17.6	28	16.7	0.25
26.0	80.0	451	18.1	13	16.0	0.39	27.1	73.8	396	17.3	28	13.1	0.32
26.0	24.0	416	18.1	27	12.9	0.32	27.1	34.8	385	17.3	21	13.4	0.30
30.3	130.9	429	16.5	13	17.2	0.40	29.6	9.8	550	17.3	18	19.6	0.31
30.3	151.6	400	16.5	23	17.4	0.26	29.6	95.2	510	17.3	17	23.9	0.34
32.0	0.1	296	15.0	15	13.3	0.31	32.1	157.7	360	18.1	13	15.8	0.48
32.9	157.2	364	18.2	18	15.4	0.32	34.7	79.3	286	18.9	16	24.0	0.38
32.5	169.9	351	17.8	12	10.9	0.36	37.0	72.6	414	17.6	13	15.9	0.31
37.3	78.9	407	15.6	16	11.7	0.37	37.0	24.2	423	17.6	15	10.6	0.47
37.3	22.2	418	15.6	20	19.3	0.38	38.8	67.3	320	16.4	11	8.5	0.45
38.5	56.7	408	16.3	11	8.6	0.41	39.7	57.8	478	17.7	19	10.6	0.24
38.5	47.1	324	16.3	12	21.5	0.32	39.7	48.1	330	17.7	14	22.5	0.38
40.8	131.2	372	16.0	19	7.7	0.36	42.6	7.9	350	17.8	8	10.7	0.47
43.0	0.5	344	15.9	15	20.0	0.45	43.0	172.0	400	16.2	16	16.0	0.32
43.0	100.3	309	15.9	17	10.8	0.39	46.1	134.9	550	17.1	7	21.5	0.47
47.5	41.9	564	19.1	10	16.8	0.36	48.5	29.0	286	16.6	8	11.3	0.36
47.5	39.3	540	19.1	8	20.9	0.29	48.5	80.5	308	16.6	6	13.4	0.58
50.3	28.7	280	15.9	5	5.2	0.48	50.0	117.6	450	16.2	6	13.2	0.34
54.6	64.5	206	18.2	6	6.2	0.26	53.0	169.0	560	16.1	4	4.6	0.35
56.6	34.4	288	18.2	5	16.5	0.25	58.0	50.0	368	18.0	6	11.9	0.55
62.4	2.8	319	17.1	5	12.1	0.23	Mean		398	17.0		15.2	0.32
Mean		406	17.0		13.3	0.30							

* Tilt angles and axes in degrees, the axes being measured relative to the [1,0] direction.
‡ Resolution in Å of first zero in contrast transfer function.
§ Number of reflections (>2× background) being compared.
‖ Average error in degrees; based on comparison of individual phases with others within 1/400 $Å^{-1}$ along the lattice lines.
¶ $\Sigma||F_i|-|F_c||/\Sigma|F_c|$, where $|F_i|$ corresponds to amplitudes of reflections (h, k) for the image being refined, and $|F_c|$ corresponds to amplitudes of reflections (h, k) for the images being compared.

posed to carbamylcholine concentrations of 100 μM and 50-fold greater yielded differences at a significance level 1% when compared with the native dataset. The differences were apparent in the same regions, relative to the projected structure, and were not present when the individual sets from the carbamylcholine-treated tubes were compared to each other. This suggested that the carbamylcholine induced a resolvable conformational change, the nature of which was indepen-

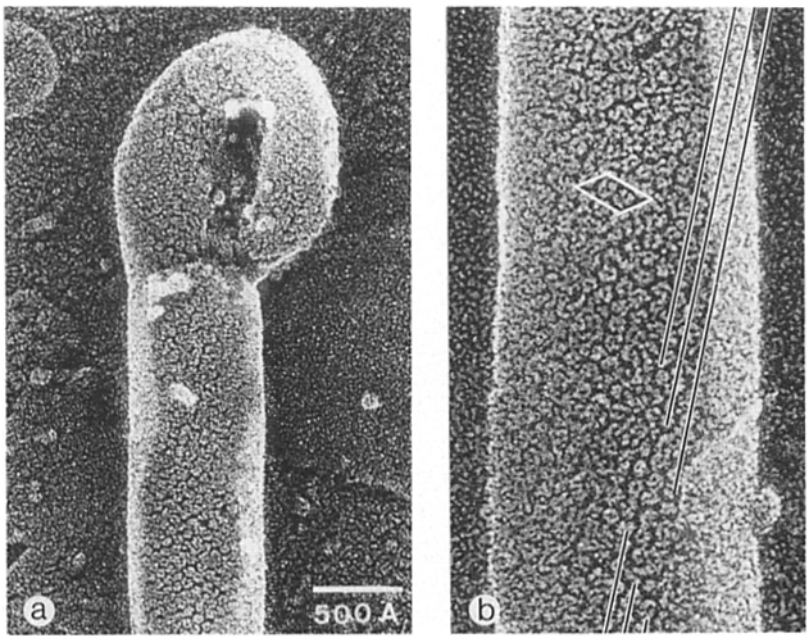

Figure 1. Outside surfaces of the crystalline tubular vesicles revealed by quick-freezing, freeze-etching and rotary shadowing (platinum-carbon at an inclination of 25°), following the procedures described in reference (4). The replicas were photographed with the electron source on the same side of the specimen as the shadow material, and printed emulsion side up so that the concealed side of the tube would be furthermost from the observer. Many of the receptors have an annular appearance due to accumulation of the platinum around the synaptic entrance to the channel. Lines in *b* identify near-axial rows of closely packed molecules pointing clockwise relative to the tube axis; the parallelogram enclosing the two receptors corresponds to the unit cell in Fig. 5.

dent of the concentration applied, at least above 100 μM. This change in projected structure was analysed further using more extensive datasets and a fixed carbamylcholine concentration of 5 mM (see below). In collecting data for the three-dimensional maps, the concentration of carbamylcholine applied was usually 200 μM.

Unit Cell and Projected Structures

Receptors are arranged on the surface lattice of the tubes in the two-sided plane group, p2 (5). Table I lists values of the unit cell parameters determined before and after exposure to carbamylcholine, and also other details (number of unit cells, defocus cut-offs, number of reflections and phase errors) illustrating that the individual images analyzed were of uniform quality, irrespective of the dataset to which they belonged. The mean (±SD) values for the unit cell parameters of the two structures were: a = 90.01 Å ± 2.30; b = 160.35 Å ± 4.12, γ = 118.85° ± 0.69 (native), and a = 91.71 Å ± 1.80; b = 159.49 Å ± 2.32; γ = 118.49° ± 0.59 (carbamylcholine-treated), indicating no detectable difference except possibly a small increase (significant at the 7% level) in the a cell dimension after exposure to carbamylcholine. In either case the value for the included angle, γ, remained relatively constant, whereas the unit cell dimensions varied considerably (by up to 6%). These variations were more marked between tubes than between the two sides composing individual tubes, suggesting that the source was a genuine packing phenomenon and not a result of interaction of the tube with the carbon support film.

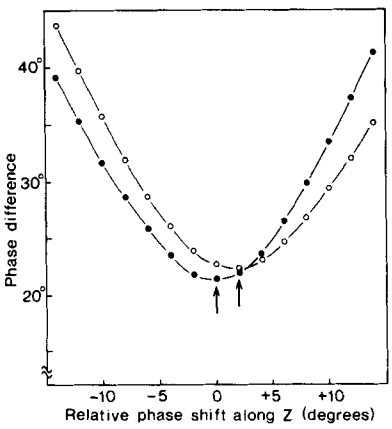

Figure 2. Alignment of the bilayer (i.e., distance along Z) with respect to the structural details, determined by plotting the average phase differences between individual datasets against relative shift in phase origin. (*Solid circles*) Comparison of the two present three-dimensional maps; (*open circles*) comparison of the new native map with the one derived previously. The positions of the two minima (*arrows*) indicate that the bilayer is equivalently located in the two present maps and shifted by ~2° (i.e., 2.2 Å) along the Z direction with respect to the previous map. Only the first five Fourier terms along each of the lattice lines were used in the calculations.

Receptors in projection maps calculated from the two datasets were similar in appearance, but not identical. The native receptor (Fig. 5 *a*) was almost symmetrical, having all five subunits extending radially toward the surrounding lipid by the same distance from the center. Exposure to carbamylcholine made the receptor less symmetrical (Fig. 5 *b*), causing the region occupied by the γ- and δ-subunits to protrude slightly further from the center. The maximum "distortion" of the structure was along the "a" direction of the unit cell (horizontal in Fig. 5 *b*), accounting for the apparent differences in this dimension. Although the change in structure was small, it was associated with a major peak in the Fourier difference map (Fig. 5 *c*), and this peak was shown to be highly significant (0.1% level) by a t test of the differences in densities between the two projection maps (Fig. 5 *d*). Other less significant changes were also evident, suggesting that the other subunits might also be implicated, but to a much lesser degree. The nature of these changes, in three-dimensions, is discussed below.

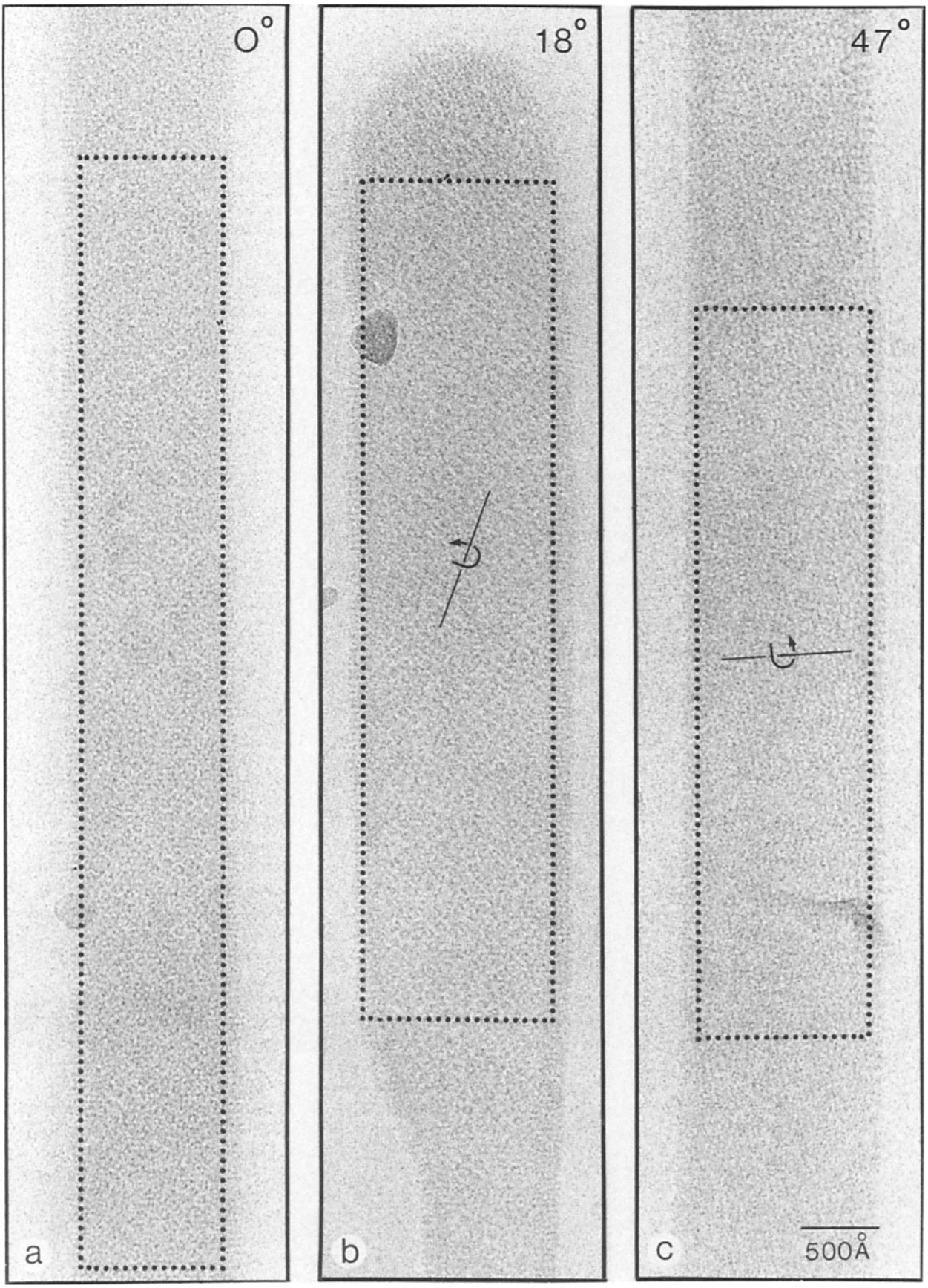

Figure 3. Images of flattened, ice-embedded native tubes tilted by: (*a*) 0°, (*b*) 18°, and (*c*) 47° to the incident electron beam. The areas boxed off for computer analysis and the directions of the tilt axes are indicated.

Figure 4. Diffraction patterns computed directly from the images. (*a–c*) From Fig. 3, *a–c*. Circles are drawn around some of the reflections arising from one side of the tube in *d*; indices for some of these reflections are indicated; the resolution of the (2, 4) corresponds to 21.8 Å. N and C refer to native and carbamylcholine-treated tubes respectively, and the figures indicate tilt angles. Diffraction patterns computed after applying the lattice corrections are sharper and contain a greater number of high resolution peaks than in these patterns. 1 cm = 0.011 $Å^{-1}$.

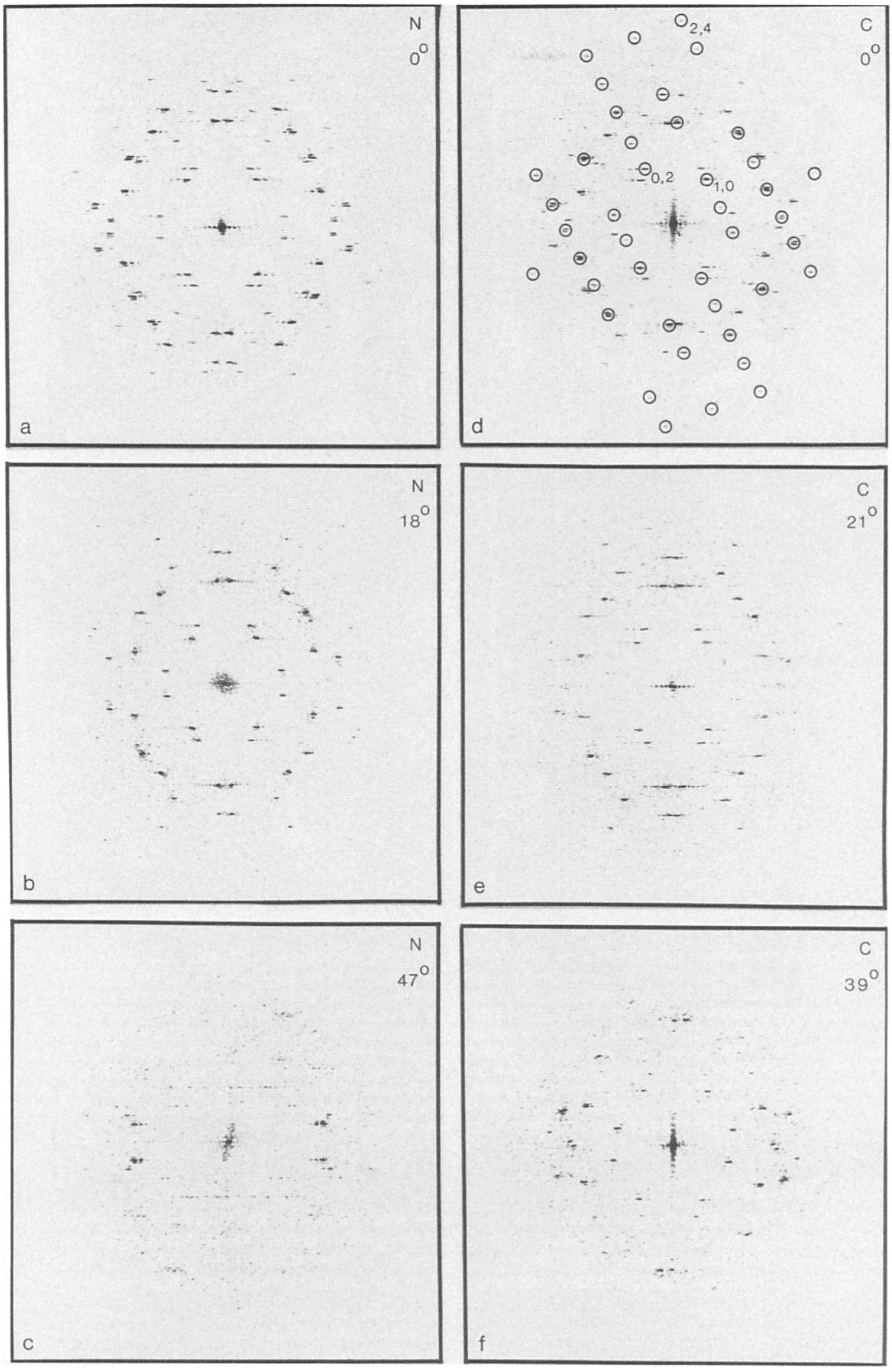

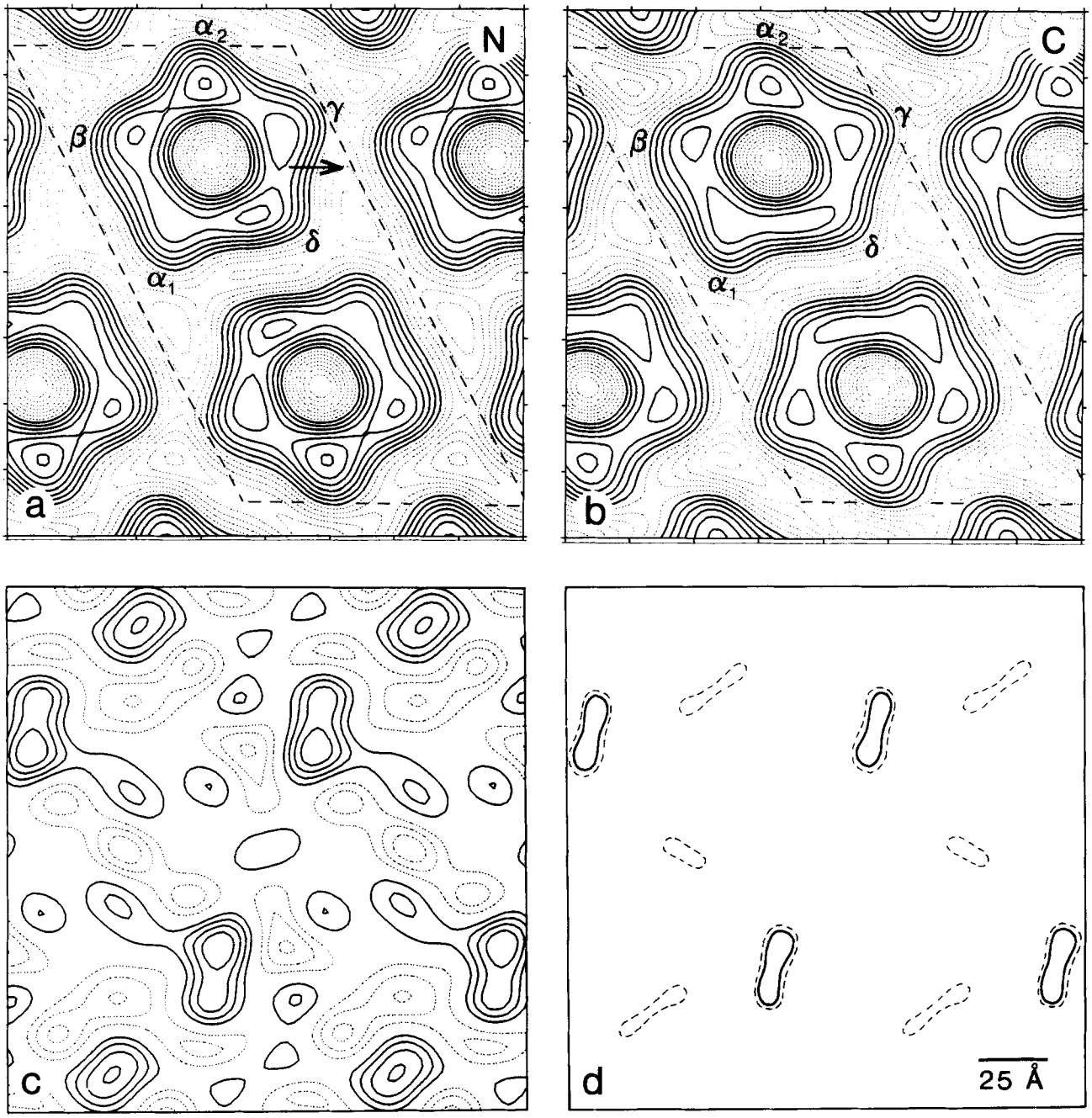

Figure 5. (*a* and *b*) Projection maps synthesized for the native (*N*) and carbamylcholine-treated (*C*) receptors, from averages of the data summarized in Table I; (*c*) Fourier and (*d*) statistical difference maps (25) calculated for the same area. The subunit assignments α_2, β, α_1, γ, and δ are as in reference 25. The region occupied by the γ- and δ-subunits protrudes slightly further from the center of the receptor after exposure to carbamylcholine, giving it a slightly distorted appearance. This distortion (indicated by the arrow in *a*) is approximately along the shorter "a" direction (horizontal) of the unit cell and appears to be responsible for the small (~1.7 Å) difference in this dimension for the two cases (see text). The Fourier difference map was synthesized assuming that the sum of the amplitudes for either structure is the same and neglects the change in unit cell dimension; positive peaks (*continuous contours*) correspond to gain of matter, and negative peaks (*dotted contours*) to loss of matter, after addition of carbamylcholine; for clarity, the zero level contour has been omitted. The statistical difference map is contoured at the 0.1% (*continuous lines*) and 1% (*broken lines*) significance levels. No compensation has been made for the effect of the contrast transfer function; the compensated maps show essentially the same features.

Three-dimensional Data

Averages of the projection data were used as reference sets in combining the images (see Materials and Methods). The rest of the data consisted of 51 sides of native tubes tilted between 5° and 62°, and 50 sides of carbamylcholine-treated tubes tilted between 5° and 58°. All these images contained similar numbers of unit cells, and were defocussed by approximately equal amounts. In addition, the variation in values for the number of reflections, phase errors and R fac-

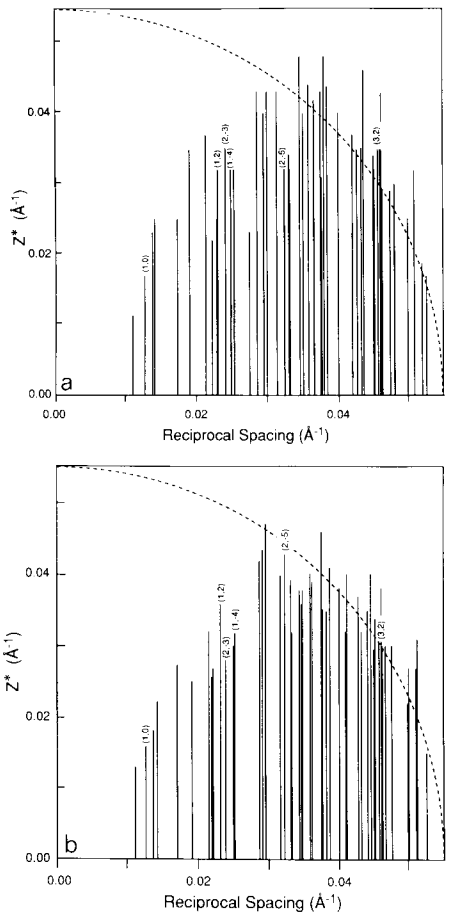

Figure 6. Extent of experimental measurements along lattice lines plotted as a function of reciprocal spacing in the plane of the bilayer: (*a*) native and (*b*) carbamylcholine-treated tubes. There are 48 lattice lines in *a* and 49 in *b*. Indices denote the lattice lines presented in Fig. 7. The arcs correspond to a resolution of 18 Å.

tors was small, indicating that the quality was quite uniform, irrespective of the treatment given (see Table II for details).

The phase and amplitude curves derived from the two datasets were determined to near the cut-off resolution (18 Å) in most instances (Fig. 6), and the missed sampling along the low resolution lattice lines (e.g. (1, 0)) due to tilt limitations, did not occur at points where the amplitudes were strong.

Fig. 7 gives examples of some typical lattice lines. The higher resolution lines, such as the (3, 2), were not generally visible in diffraction patterns before correction for lattice distortions. Although the differences between corresponding amplitude and phase curves for native and carbamylcholine-treated tubes when considered individually were small, they combined additively to produce significant differences in the resultant maps (see below).

Fourier Maps

Maps of the two structures were synthesized after compensating the low resolution Fourier terms for the effect of the CTF (see Materials and Methods) and displayed as sets of equally spaced sections parallel to the plane of the bilayer. The individual subunits were most well resolved in the portion identified previously (6) as the bilayer-spanning portion.

Fig. 8 *a* illustrates the appearance of the two structures and traces the paths followed by the peaks identifying the subunits within this region. The subunits were arranged here symmetrically about the channel, but with small differences in their individual alignments. The differences in path between the two structures were least for the β- and two α-subunits and greatest for the γ- and δ-subunits. After exposure to carbamylcholine, the path followed by the γ-subunit was at higher radius (by ~2 Å), whereas the path followed by the δ-subunit was inclined slightly in the opposite direction.

These changes in radius and angle of the γ- and δ-subunits affected their intermolecular associations, as they were noticeably closer to the juxtaposed β- and δ-subunits of neighboring molecules after exposure to the carbamylcholine (Fig. 8 *a*). The α_1-α_1 and α_2-α_2 associations, at this level of the structure, appeared not to be affected.

We used equivalent sets of sections from the bilayer-spanning portion to evaluate the significance of various features. To assess the influence of the CTF, maps were also calculated from the uncompensated datasets (Fig. 8 *b*). In this case the individual subunits were more clearly resolved, but still showed the same qualitative similarities between the β- and two α-subunits and differences between the γ- and δ-subunits. On the other hand, the apparent diameter of the channel increased, suggesting that the maps do not give an accurate representation of dimensional aspects of the structure. In another test, the image datasets were each divided in two (selecting alternative images from the list in Table II) and processed independently to derive new amplitude and phase curves fitted to only half the total number of data points. Maps obtained this way (Fig. 8, *c* and *d*) again showed essentially the same similarities and differences in the arrangement of the subunits. Since neither the CTF nor statistical limitations in the data have an important influence on these positional features, it is most likely that they reflect genuine, distinctive properties of the two structures.

Pentagonal Symmetry

The pentagonal symmetry was evaluated in successive sections parallel to the plane of the bilayer (Fig. 9; see Materials and Methods). As found previously (6), it was most perfect at the central core of the bilayer and over a contiguous region on the synaptic side. However, the symmetry fell off more rapidly on either side of the bilayer in the case of the carbamylcholine-treated receptor.

Surface Features

Wooden models of the native and carbamylcholine-treated receptors were constructed to provide an overall molecular picture. The surfaces of these models were made to correspond to the outermost contours in the Fourier maps (the zero level; Fig. 8 *a*) and incorporated all sections for which the contrast (measured as the difference between the maximum and minimum densities) was greater than 25% of the value at the middle. These cut-off criteria gave a total volume close to the value of 350,400 $Å^3$ expected for the glycosylated protein (26).

Inspection of both models (Figs. 10 and 11) showed that the subunit surfaces, although displaying certain individual characteristics, had a number of basic features in common.

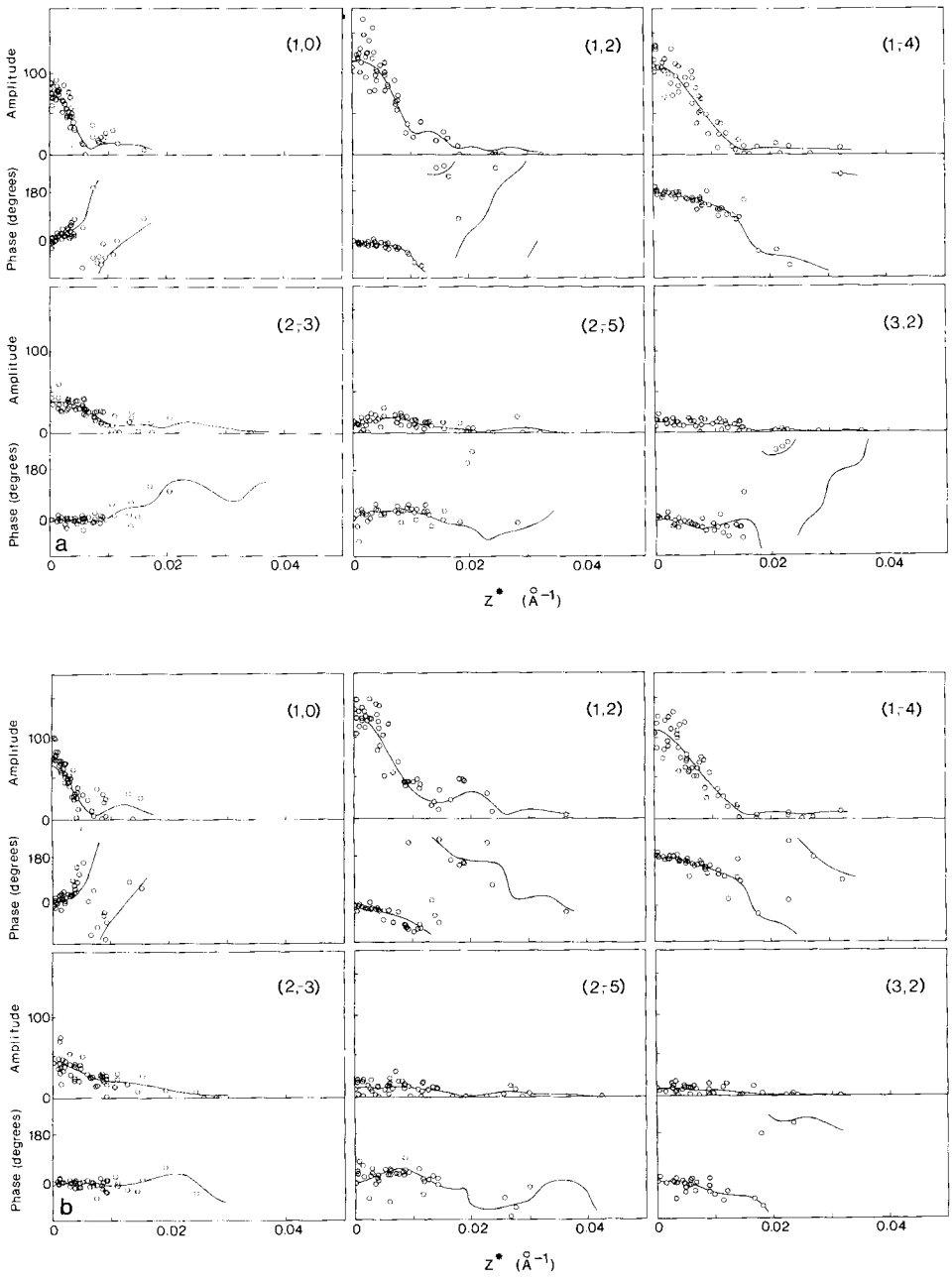

Figure 7. Experimental values and calculated curves tracing the continuous variation of amplitude and phase as a function of distance, Z^*, along some typical lattice lines; native (*a*) and carbamylcholine-treated tubes (*b*). The curves in either case are very similar; the (1, 2) lattice lines differ the most.

In particular, they each formed a distinct ridge within the bilayer portion which broadened toward the synaptic end (uppermost).

The two models were most alike when viewed with the β-subunit facing the observer (Fig. 10). From this direction the grooves between the facing (β) and adjacent (α) ridges, and the overall outlines of the two receptors matched up quite closely. Only at the cytoplasmic ends (bottom), where other material may be present (see Discussion) were the similarities less clear and features more difficult to reconcile.

Face-on views of either α-subunit (not shown) also resembled one another, and indeed the whole α_1-β-α_2 side of the

Figure 8. Equivalent portions of the two three-dimensional maps extending over most of the bilayer-spanning region of a single molecule (see Figs. 10 and 11), obtained by stacking on top of one another successive sections parallel to the bilayer plane; (*left*) native receptor; (*right*) carbamylcholine-treated receptor. The interval between sections corresponds to 5 Å, and dots at the peak positions at each level trace the paths taken by the individual subunits. The view is from the synaptic side. Negative contours have been omitted, and only the zero level and positive contours are shown. (*a*) Structures with compensations applied to the low resolution Fourier terms assuming 15% amplitude contrast (see Materials and Methods); individual subunits of the central receptor (*large lettering*) and of neighboring molecules (*small lettering*) are identified (25); (*b*) structures with no compensation applied; *c* and *d* contain the same compensations as *a*, but are independently determined structures calculated from alternative halves of the original image datasets.

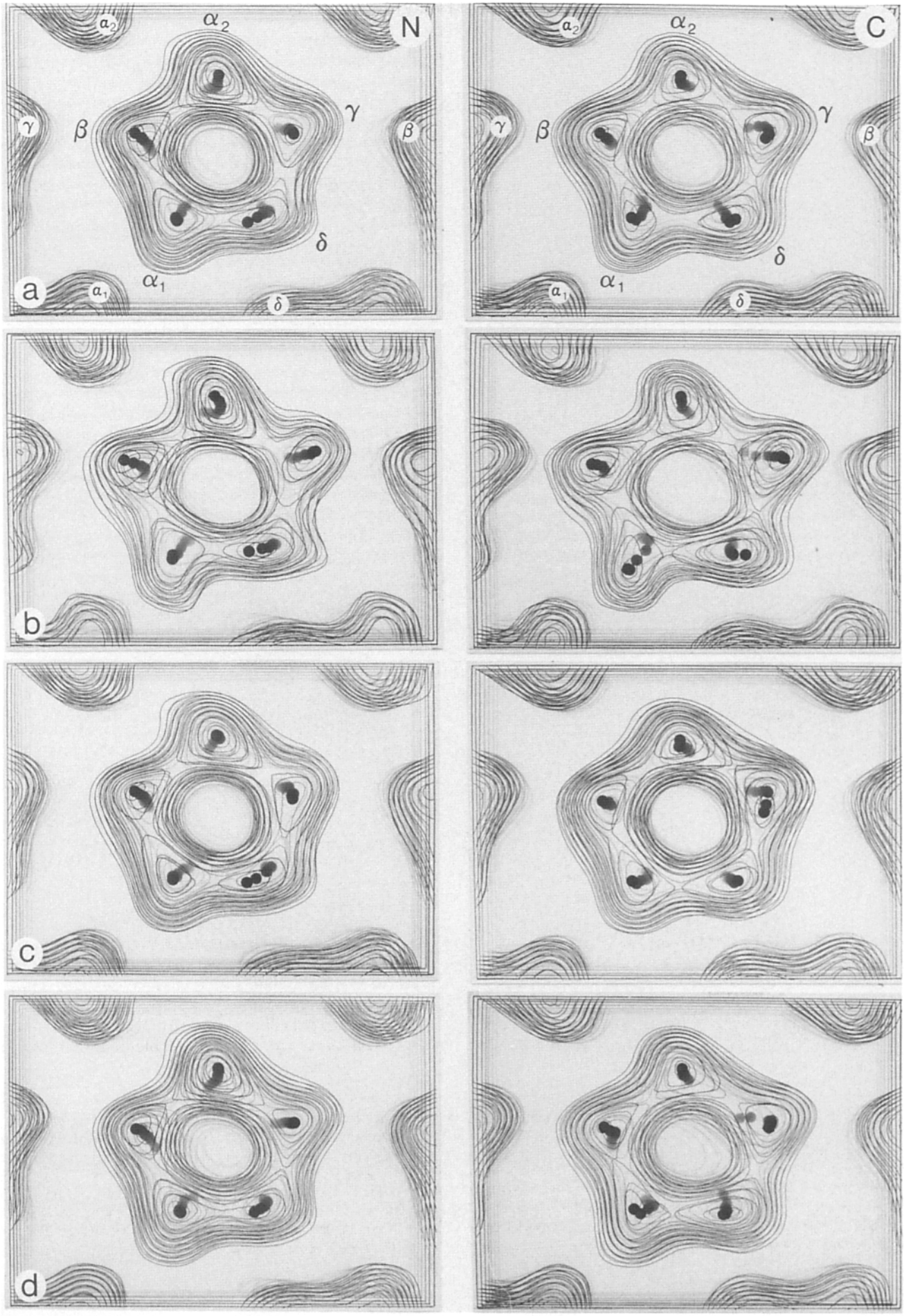

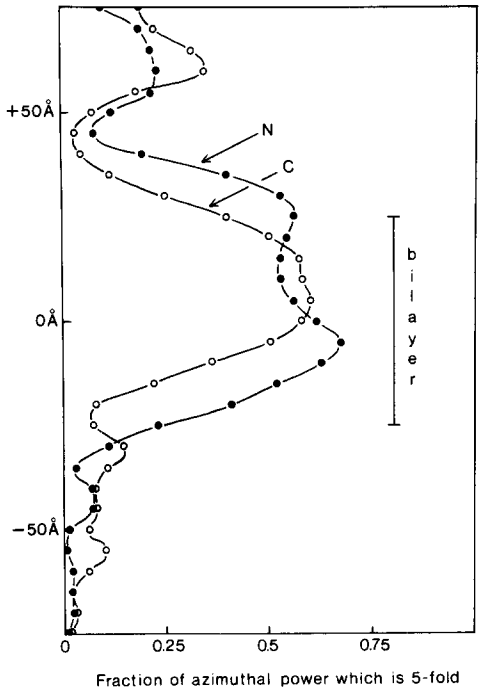

Figure 9. Fraction of azimuthal power which is fivefold for single native (*N*) and carbamylcholine-treated (*C*) receptors, plotted as a function of distance perpendicular to the bilayer plane. The calculations are made from sections at 5-Å intervals through the two three-dimensional maps. The location of the bilayer is indicated; the synaptic end is uppermost.

two receptors showed good correspondence, except for the small portion extending into the cytoplasm.

The δ- and γ-subunit surfaces changed the most on exposure to carbamylcholine (Fig. 11). The ridge formed by the δ-subunit (equivalent points marked by dotted lines) became more steeply inclined tangential to the axis of the receptor, producing noticeable changes in the appearance of the receptor's uppermost face (*upper pair*) and profile (*lower pair*). The γ-subunit surface was less affected, but consistent with the details in Figs. 5 and 8, became slightly more distant from the receptor axis over much of its length (compare profiles in upper pair, Fig. 11).

Subunit Configurations in Radial Projection

A disadvantage of the wooden models is that they give only a qualitative picture of the subunit configurations: at low resolution, surface features are influenced by the nature of the associations between neighboring molecules and, as pointed out above, these were not identical in the two maps. To obtain a more quantitative indication of the configurations it was necessary to examine the densities representing the main masses of the subunits. We therefore calculated radial projections of the two structures, by superimposing successive cylindrical sections concentric about the receptor axis (see Materials and Methods).

Fig. 12 illustrates the two structures in radial projection. Most striking in this representation were the pronounced differences in inclination of the densities corresponding to the δ-subunit, yet fairly consistent orientation of the densi-

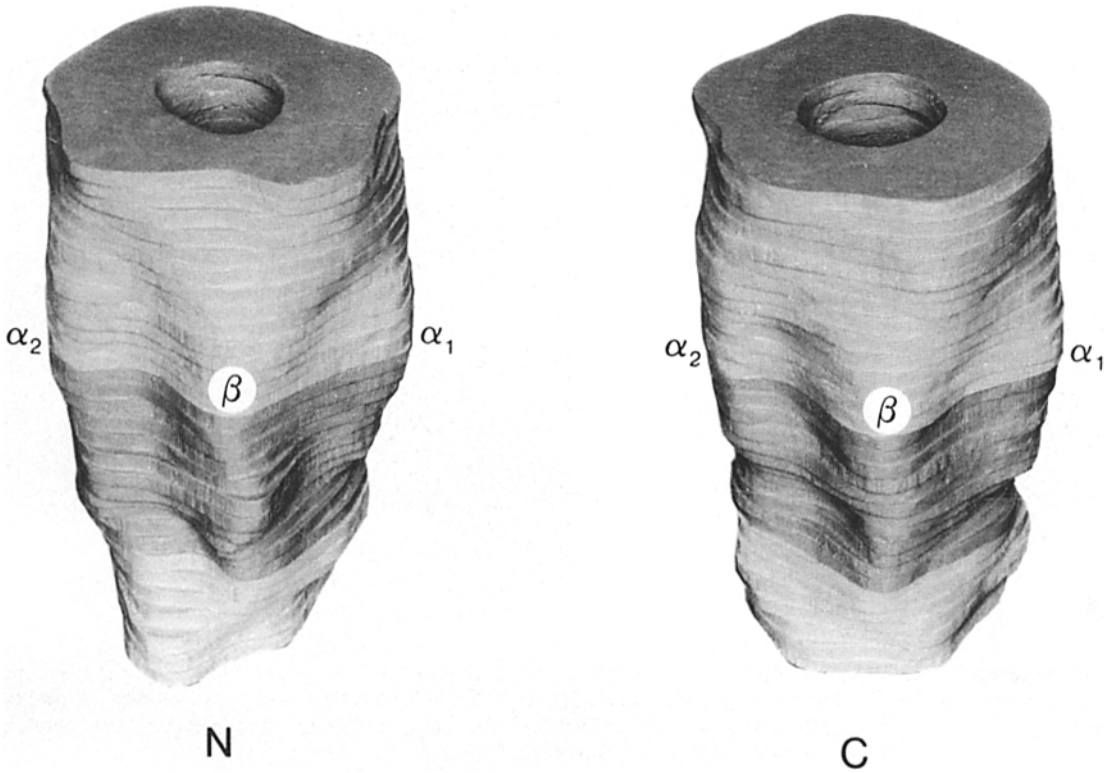

Figure 10. Balsa-wood models of the acetylcholine receptor before (*N*) and after (*C*) exposure to carbamylcholine, looking toward the face of the β-subunit (synaptic end uppermost). Both structures share very similar features when viewed in this direction. The cut-out level in this figure and Fig. 11 correspond to the zero density level (i.e., the outermost contour of Fig. 8 *a*). The thickness of the individual slabs corresponds to 4 Å, and the darker shadowing around the lower-middle portion of the molecule indicates the portion that would be in contact with the lipid bilayer (assumed 50-Å wide).

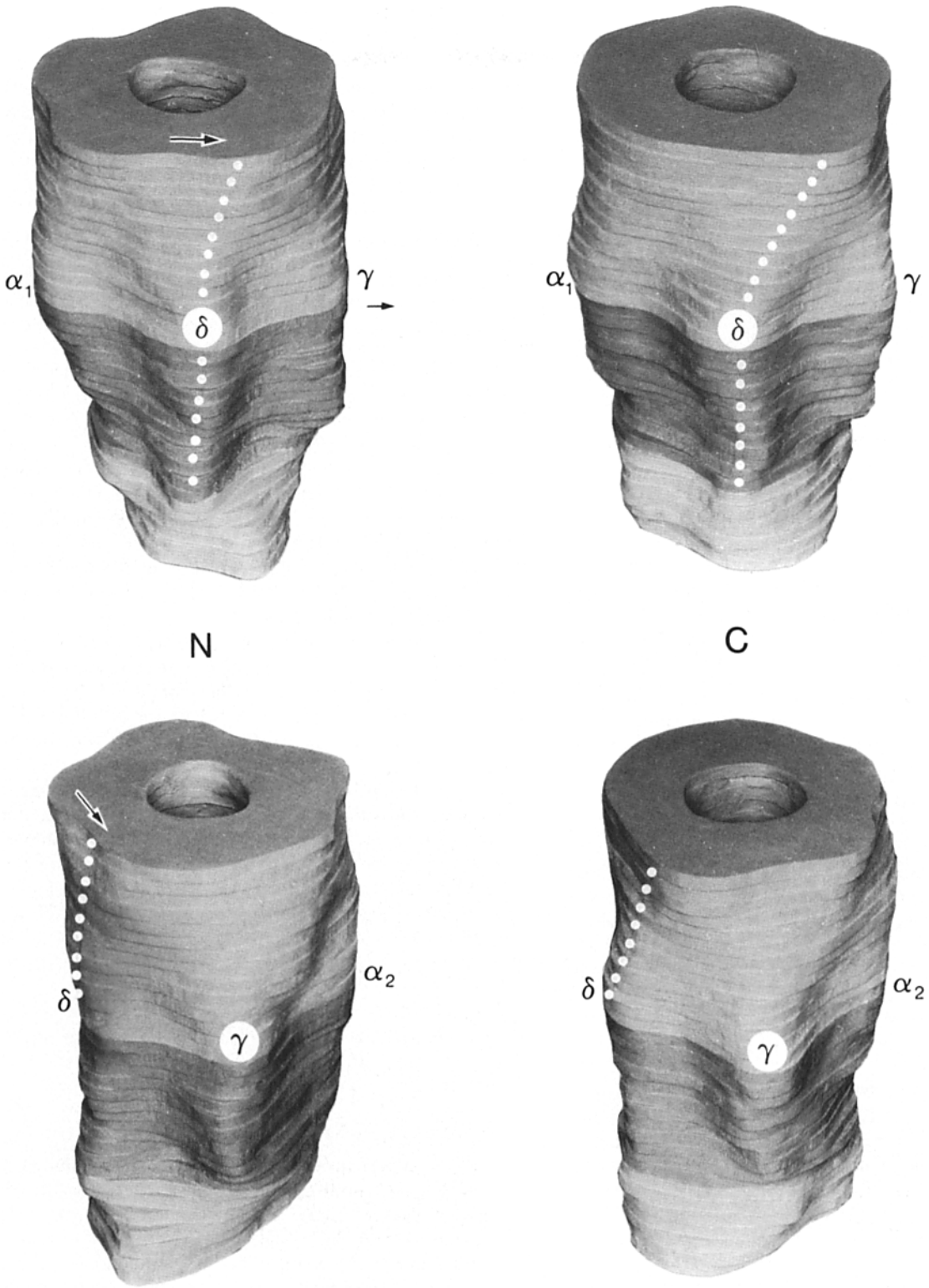

Figure 11. The acetylcholine receptor before (*N*) and after (*C*) exposure to carbamylcholine, looking toward the faces of the δ-subunit (*upper pair*) and γ-subunit (*lower pair*). The δ-subunit changes its tilt tangential to the axis of the receptor on exposure to carbamylcholine (indicated by the dotted lines following a clearly delineated ridge, and arrows). The γ-subunit, at the same time, moves radially outward (indicated by the small horizontal arrow relating the two profiles at the top of the figure).

ties corresponding to other subunits. In the native receptor the main mass of the δ-subunit followed a path (*broken line*) which, overall, was like that of the other subunits (i.e., approximately perpendicular to the bilayer plane), whereas in the carbamylcholine-treated receptor the main mass of this subunit followed a path which was inclined strongly to the right, in misalignment with the other four subunits. These differences in inclination of the δ-subunit were not revealed

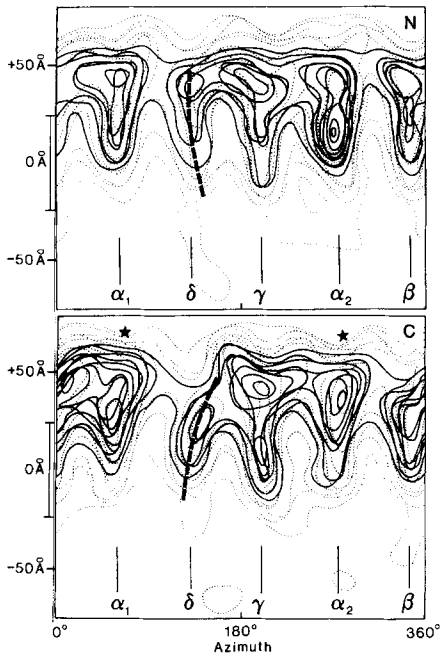

Figure 12. Radial projections of the native (*N*) and carbamylcholine-treated (*C*) receptor, obtained by superimposing cylindrical sections calculated for radii of 25, 28, 31, and 34 Å. The view is from the outside toward the central axis, with the synaptic end uppermost. The two distinct inclinations of the δ-subunit are indicated by the broken lines. The continuous contours enclose the higher density regions of individual subunits. The location of the lipid bilayer (see Figs. 9–11) is indicated on the side. The carbamylcholine is presumed to bind to the α-subunits at their synaptic ends (*stars*; [24, 25]).

at either extremity of the receptor, but clearly extended from the synaptic portion (as emphasized by the wooden models) across the bilayer. The change in tilt over this region corresponded to ~10°, and was about a radial axis located at the level of the bilayer (since the δ-subunit retained the same azimuth in this part of either structure). The loss in subunit alignment due to tilting of the δ-subunit appears to be the main factor responsible for the more rapid fall-off in pentagonal symmetry of the receptor in the presence of carbamylcholine (Fig. 9).

Fig. 12 also suggests that the carbamylcholine may have induced more localized distortions of some of the subunits (for example, of the β- and 2 α-subunits near their synaptic ends); however we have not established that these smaller apparent changes are significant.

Discussion

Earlier work on the tubular crystals demonstrated that they consist of biochemically intact receptors, surrounded by native lipid molecules and linked to each other through disulphide bonds between their δ-subunits (5, 25). The five subunits were identified individually (25) and seen to be aligned symmetrically around the central ion channel in an orientation approximately perpendicular to the bilayer plane (6). In the present study we have used improved procedures of data acquisition and processing (see Materials and Methods) to explore the structure of the receptor in finer detail and to examine the structural change produced by exposing the crystals to an acetylcholine analogue, carbamylcholine, under conditions that would be expected to induce final stabilization of the receptor in the doubly liganded desensitized state (23, 27). Our results confirm the basic structural features seen at lower resolution previously and allow a description of the carbamylcholine-induced structural change in terms of quaternary rearrangements of the individual subunits.

Three-dimensional Structure

At 18 Å resolution, the receptor presented a similar overall appearance as in the earlier study (6). It has an angular shape, contained within a 65–70 Å diameter and ~140 Å long cylindrical shell. However, we could now resolve peaks in the contour maps which traced unambiguously the paths followed by each subunit throughout the bilayer-spanning portion (Fig. 8). The subunits followed similar, but not exactly equivalent paths within this portion, leading to good pentagonal symmetry (Fig. 9), consistent with their amino-acid homology and putative transmembrane α-helical conformation (reviewed in 28). In the synaptic portion the subunits were also more easily distinguished, although the narrow ridge created by their surfaces within the bilayer (Figs. 8, 10, and 11) became broader and less distinct towards the synaptic end (Figs. 10 and 11), making their exact locations less certain. As before (6), the subunits could not be distinguished individually near the cytoplasmic end of either structure, and the present study does not provide additional information about this region. It is possible that the matter near the cytoplasmic end of the receptor is at least in part composed of the 43kD and/or other endogenous protein (12). This material appears to bind to the extremity of the receptor, since it increases the thickness of the stain layer adjacent to the membrane in thin-sectioned postsynaptic membranes (30) and increases the height of the protrusions revealed on the cytoplasmic surfaces by freeze-etching (4). The cytoplasmic portion of the carbamylcholine-treated receptor occupied a greater apparent volume than that of the native receptor (Figs. 10 and 11), reflecting perhaps a slightly more ordered conformation.

The shape of the central ion channel could not be evaluated more accurately than in the earlier study because of similar limitations in specimen tilt (see Table II), the effect of which is to blur detail along the receptor axis.

Description of the Quaternary Rearrangement

We found that exposure of the crystals to carbamylcholine at concentrations of 100 μM and greater led to small, but significant changes in projected structure of the receptor in the region of its δ- and γ-subunits (Fig. 5). The origin of these changes became apparent after comparison of the three-dimensional details. First, from successive sections spanning the bilayer portion of the structures (Fig. 8) the carbamylcholine was seen to induce small changes in the paths traced by the δ- and γ-subunits: the δ-subunit changed its tilt tangential to the receptor axis, and the γ-subunit moved to a slightly higher radius. Second, from comparison of wooden models of the two receptors (Fig. 11), corresponding changes were observed in the surface features, which extended beyond the bilayer into the synaptic portion of the structure. Third, from radial projections calculated about the

receptor axis (Fig. 12), it was evident that the carbamylcholine induced marked displacements of the densities associated with the δ-subunit over a large fraction of its length; the displacements increased with distance from the bilayer, indicating a change of tilt, tangential to the receptor axis, of ~10°. Thus the tangential displacement of the δ-subunit and, to a lesser degree, the radial displacement of the γ-subunit represented the most extensive structural responses elicited by the carbamylcholine.

In contrast, the remaining (α- and β-) subunits were more tightly linked together, appearing to act as a wall against which the movements of the γ- and δ- subunits were facilitated. There may well have been small localized distortions of the β- and two α- subunits near the synaptic end of the liganded structure (see Fig. 12) and these may have accompanied the binding of the carbamylcholine, triggering the longer range displacements. A concerted interaction of this kind would be consistent with the allosteric properties of this molecule (8); however, the finer, localized detail could not be interpreted with confidence.

Relation to Other Work

The rearrangements of the γ- and δ-subunits are, to some extent, analogous to those of the subunits of the gap junction channel when exposed to physiological stimuli (34). With both oligomers the displacements are such as to maintain essentially the same hydrophobic protein surfaces in contact with the hydrophobic lipid chains. The motions are predominantly within the plane of the bilayer, rather than perpendicular to it, and the tilting of the δ-subunit is about an axis which minimizes relative movement in the bilayer-spanning portion of the structure. An additional aspect of the conformational change of the receptor, however, is that the subunits do not participate in an equal way. As a result the structure switches less concertedly, and from a more symmetrical (resting) to a less symmetrical (desensitized) configuration. It is likely that some localized distortion of the subunits represents an important component of this action.

It is interesting that the δ-subunit appears to play a key structural role in desensitization, given that the kinetics of the process is modulated by its state of phosphorylation (21, 26). The importance of the δ-subunit in channel gating has also been emphasized in electrophysiological experiments on hybrid calf/*Torpedo* receptors obtained by expression of substituted mRNAs in *Xenopus* oocytes (29). More recently, the conductance properties attributable to the δ-subunit have been localized to a region including the putative transmembrane α-helix, M2 (22).

The implication of the γ-subunit in the structural transition is corroborated by experiments with noncompetitive antagonists which label homologous residues on M2 of the different subunits, and therefore appear to interact with the subunits in the region of the ion channel itself. Triphenylmethylphosphonium, for example, shows a weaker photolabeling affinity for the γ- than the other chains (20); chlorpromazine shows slower labeling kinetics for this chain of receptors which have been preincubated with acetylcholine (15, 16). Both probes promote desensitization (7, 31) and therefore favour displacement of the γ-subunit away from the axis of the channel. Such a displacement could be responsible for their weaker reactivity with the γ-chain.

We thank Sue Whytock for help with the heavy metal shadowing experiment (Fig. 1). C. Toyoshima is a Muscular Dystrophy Association postdoctoral fellow.

This research was supported by grants GM2764 and GM30387 from the National Institutes of Health.

Received for publication 21 April 1988, and in revised form 7 June 1988.

References

1. Amos, L. A., R. Henderson, and P. N. T. Unwin. 1982. Three-dimensional structure determination by electron microscopy of two-dimensional crystals. *Prog. Biophys. Mol. Biol.* 39:183–231.
2. Agard, D. A. 1983. A least-squares method for determining structure factors in three-dimensional tilted-view reconstructions. *J. Mol. Biol.* 167: 849–852.
3. Barrantes, F. J. 1978. Agonist-mediated changes of the acetylcholine receptor in its membrane environment. *J. Mol. Biol.* 124:1–26.
4. Bridgman, P. C., C. Carr, S. E. Pedersen, and J. B. Cohen. 1987. Visualization of the cytoplasmic surface of the *Torpedo* postsynaptic membranes by freeze-etch and immuno-electron microscopy. *J. Cell Biol.* 105:1829–1846.
5. Brisson, A., and P. N. T. Unwin. 1984. Tubular crystals of acetylcholine receptor. *J. Cell Biol.* 99:1202–1211.
6. Brisson, A., and P. N. T. Unwin. 1985. Quaternary structure of the acetylcholine receptor. *Nature (Lond.).* 315:474–477.
7. Carp, J. S., R. S. Aronstam, B. Witkop, and E. X. Albuquerque. 1983. Electro-physiological and biochemical studies on enhancement of desensitization by phenothiazine neuroleptics. *Proc. Natl. Acad. Sci. USA.* 80: 310–314.
8. Changeux, J.-P., A. Devillers-Thiery, and P. Chemouilli. 1984. Acetylcholine receptor: an allosteric protein. *Science (Wash. DC).* 225:1335–1345.
9. Crowther, R. A., and L. A. Amos. 1971. Harmonic analysis of electron microscope images with rotational symmetry. *J. Mol. Biol.* 60:123–130.
10. Dubochet, J., J. Lepault, R. Freeman, J. A. Berriman, and J.-C. Homo. 1982. Electron microscopy of frozen water and aqueous solutions. *J. Microsc.* 128:219–237.
11. Erickson, H. P., and A. Klug. 1973. Measurement and compensation of defocusing and aberrations by Fourier processing of electron micrographs. *Phil. Trans. Roy. Soc. Ser. B.* 261:105–118.
12. Froehner, S. C. 1986. The role of the postsynaptic cytoskeleton in AchR organization. *Trends in Neurosci.* 9:37–41.
13. Grunhagen, H. H., and J.-P. Changeux. 1976. Studies on the electrogenic action of acetylcholine with *Torpedo marmorata* electric organ V. Qualitative correlation between pharmacological effects and equilibrium process of the cholinergic receptor protein as revealed by the structural probe quinacrine. *J. Mol. Biol.* 106:517–535.
14. Hamilton, S. L., D. R. Pratt, and D. C. Eaton. 1985. Arrangement of the subunits of the nicotinic acetylcholine receptor of *Torpedo californica* as determined by α-neurotoxin cross-linking. *Biochemistry.* 24:2210–2219.
15. Heidmann, T., and J.-P. Changeux. 1984. Time-resolved photolabeling by the noncompetitive blocker chlorpromazine of the acetylcholine receptor in its transiently open and closed ion channel conformations. *Proc. Natl. Acad. Sci. USA.* 81:1897–1901.
16. Heidmann, T., and J.-P. Changeux. 1986. Characterization of the transient agonist-triggered state of the acetylcholine receptor rapidly labeled by the noncompetitive blocker [^{3}H] chlorpromazine: additional evidence for the open channel conformation. *Biochemistry.* 25:6109–6113.
17. Henderson, R., J. M. Baldwin, K. H. Downing, J. Lepault, and E. Zemlin. 1986. Structure of purple membrane from *Halobacterium halobium*: recording, measurement and evaluation of electron micrographs at 3.5 Å resolution. *Ultramicroscopy.* 19:147–178.
18. Henderson, R., and P. N. T. Unwin. 1975. Three-dimensional model of purple membrane obtained by electron microscopy. *Nature (Lond.).* 257: 28–32.
19. Hess, G. P., and J. B. Udgaonkar. 1987. Chemical kinetic measurements of transmembrane processes using rapid reaction kinetics: acetylcholine receptor. *Annu. Rev. Biophys. Chem.* 16:507–534.
20. Hucho, F., W. Oberthür, and F. Lottspeich. 1986. The ion channel and the nicotinic acetylcholine receptor is formed by the homologous helices MII of the receptor subunits. *FEBS (Fed. Eur. Biochem. Soc.) Lett.* 205:137–142.
21. Huganir, R. L., A. H. Delcour, P. Greengard, and G. P. Hess. 1986. Phosphorylation of the nicotinic acetylcholine receptor regulates its rate of desensitization. *Nature (Lond.).* 321:774–776.
22. Imoto, K., C. Methfessel, B. Sakmann, M. Mishina, Y. Mori, T. Konno, K. Fukuda, M. Kurasaki, H. Bujo, T. Fujita, and S. Numa. 1986. Location of a δ-subunit region determining ion transport through the acetylcholine receptor channel. *Nature (Lond.).* 324:670–674.
23. Karlin, A. 1980. Molecular properties of nicotinic acetylcholine receptors.

In The Cell Surface and Neuronal Function. C. W. Cotman, G. Poste, and G. L. Nicolson, editors. 191–260.
24. Kistler, J., R. M. Stroud, M. W. Klymkowski, R. A. Lalancette, and R. H. Fairclough. 1982. Structure and function of an acetylcholine receptor. *Biophys. J.* 37:371–383.
25. Kubalek, E., S. Ralston, J. Lindstrom, and N. Unwin. 1987. Location of subunits within the acetylcholine receptor by electron image analysis of tubular crystals from *Torpedo marmorata*. *J. Cell Biol.* 105:9–18.
26. Miles, K., D. T. Anthony, L. L. Rubin, P. Greengard, and R. L. Huganir. 1987. Regulation of nicotinic acetylcholine receptor phosphorylation in rat myotubes by forskolin and cAMP. *Proc. Natl. Acad. Sci. USA.* 84: 6591–6596.
27. Neubig, R. R., and J. B. Cohen. 1979. Equilibrium binding of [^{3}H] tubocurarine and [^{3}H] acetylcholine by *Torpedo* postsynaptic membranes. Stoichiometry and ligand interactions. *Biochemistry.* 18:5464–5475.
28. Popot, J.-L., and J.-P. Changeux. 1984. The nicotinic receptor of acetylcholine: structure of an oligomeric integral membrane protein. *Physiol. Rev.* 64:1162–1239.
29. Sakmann, B., C. Methfessel, M. Mishina, T. Takahashi, T. Takai, M. Kurasaki, K. Fukuda, and S. Numa. 1985. Role of acetylcholine receptor subunits in gating of the channel. *Nature (Lond.).* 318:538–543.
30. Sealock, R. 1982. Cytoplasmic surface structure in postsynaptic membranes from electric tissue visualized by tannic-acid-mediated negative contrasting. *J. Cell Biol.* 92:514–522.
31. Spivak, C. E., and E. X. Albuquerque. 1985. Triphenylmethylphosphonium blocks the nicotinic receptor noncompetitively. *Mol. Pharmacol.* 27:246–255.
32. Thon, F. 1966. Zue Defokussierungsabhaengigkeit des Phasenkontrastes bei der elekronenmikroskopischen Abbildung. *Z. Naturforschg.* 21*a*: 476–478.
33. Toyoshima, C., and P. N. T. Unwin. 1988. Contrast transfer for frozen-hydrated specimens: determination from pairs of defocused images. *Ultramicroscopy.* In press.
34. Unwin, P. N. T., and P. D. Ennis. 1984. Two configurations of a channel-forming membrane protein. *Nature (Lond.).* 307:609–613.
35. Unwin, P. N. T., and R. Henderson. 1975. Molecular structure determination by electron microscopy of unstained crystalline specimens. *J. Mol. Biol.* 94:425–440.
36. Wrigley, N. G. 1968. The lattice spacing of crystalline catalase as an internal standard of length in electron microscopy. *J. Ultrastruct. Res.* 24: 454–464.